UNIVERSITY OF VICTORIA
Department of Electrical and Computer Engineering

Compressive Sensing for Sparse Recovery in Phase Shift Depth Migration based Plane Wave Ultrasound Imaging.

ECE 573 Advanced Engineering Design by Optimization

PROJECT REPORT
Submitted by

Derrell D'Souza (V00901532)

April 13th, 2019

ABSTRACT

Plane Wave Ultrasound Imaging is an important modality which enables very high frame rates for adequate characterization of tissue and blood flow properties. This work describes compressive sensing based sparse signal recovery for a novel Fourier domain Plane Wave Ultrasound image reconstruction algorithm. The approach is based on scaled ADMM iterations for compressive sensing first in spatial domain and then in time domain. In time domain, we aim to use compressed sensing to reduce the sampling rate of Analog to Digital Converter i.e. number of samples received by each transducer element in the array. In spatial domain, we use compressed sensing to compress an array of large number of transducer elements into an array of much smaller number of transducer elements. We perform several experiments involving complete recovery and individual spatial and temporal recovery.

I. Introduction

Ultrasound (US) imaging is one of the most commonly used medical imaging modalities. Its low cost, non-ionizing characteristics, ease of use and real-time nature make it the gold standard for many crucial diagnostic examinations [1]. In plane wave ultrasound imaging plane waves are used to insonify a very large field of view in a single transmission and then building an image from the resulting backscattered echoes [2]. The clinical ultrasound is based on a similar acoustical echo method where the part of the body under examination is insonified with an acoustic pulse that gets reflected and scattered by the variations in density of the issues along the propagation path. These reflected signals, which carry the information about the mechanical properties of the body, are then received by piezoelectric sensors. The image is extracted from the received signals by averaging them after supplying appropriate set of delays determined by the geometric paths between the field points and transducers [3].

The novel plane-wave image reconstruction method considers vertical (depth-dependent) velocity variations in a horizontally stratified medium. Here, the approach is based on the geophysical concept of zero-offset phase-shift migration under the exploding-reflector model (ERM) assumptions where instead of considering two-way wave propagation along the vertical z-axis (from a given surface transmitter down to a subsurface reflector and then back up to a surface receiver at the same location), the original model considers only one way upward propagation at half-speed (from an "exploding "reflector to the receiver in question), while allowing the speed values to vary with depth [4].

Compressed sensing is a technique to sample compressible signals below the Nyquist rate, whilst still allowing near optimal reconstruction of the signal. Instead of taking samples at the Nyquist rate, compressed sensing uses linear sampling operators that map the signal into a small (compared to the Nyquist rate) dimensional space, whilst reconstruction of the signal is highly non-linear [5]. Compressive sensing differs from compression as the signal is directly acquired or sampled in its compressed form [6]. With the help of Compressed sensing (CS) we can now reconstruct signals and images from significantly fewer measurements than were traditionally thought necessary.

Compressive sensing is benefiting to ultrasound imaging which is an essential medical imaging tool with an inherently slow data acquisition process. In ultrasound imaging, the amount of data can be a limiting factor for real-time imaging or simply data storage. Applying CS to Ultrasound Imaging offers potentially significant scan time reductions, with benefits for patients and health care economics. It can also offer potential significant hardware reductions by reduction in size of sensor array. Ultrasound Imaging obeys two key requirements for

successful application of CS: 1) medical imagery is naturally compressible by sparse coding in an appropriate transform domain (e.g., by wavelet transform), and 2) Ultrasound scanners naturally acquire encoded samples, rather than direct pixel samples (e.g., in spatial-time encoding) [7]. However, because the underlying signal is compressible, the nominal number of signal samples is a gross overestimate of the "effective" number of "degrees of freedom" of the signal. As a result, the signal can be reconstructed with good accuracy from relatively few measurements by a nonlinear procedure.

II. Theoretical Background and Problem Formulation

A. Raw RF Data generation and its preprocessing

For the problem at hand we have used the K-WAVE MATLAB toolbox to simulate signal acquisition [8] under the following assumptions:

A 128-element linear transducer (0.308-mm pitch) emits a 2-MHz plane-wave Gaussian pulse (wavelength λ = 0.770 mm, 4.5 cycles), which propagates through a three-layer medium towards ball-shaped "point" targets (0.616-mm diameter) located at the following (x,z) coordinates as specified in Table 1. We have simulated Plane Wave emissions using 0^0 angle [4].

Upper targets	$(-13,22), (0,22), (13,22)$ mm.
Middle targets	$(-13,35), (0,35), (13,35)$ mm.
Lower targets	$(-13,48), (0,48), (13,48)$ mm.

Table 1. Location of point targets [4]

The propagation medium properties are specified in Table 2 mimicking an approximate tissue-bone-tissue layer arrangement.

Medium Layer	Speed c_z, m/s	Density kg/m^3	Abs. coeff dB/cm- MHz	Depth Span mm
I	1540	1000	0.75	$0 < \mathrm{z} < 5$
II	3198	1990	3.54	$5 \leq \mathrm{z} < 12$
III	1540	1000	0.75	$12 \leq \mathrm{z} < 63$

Table 2. Propagation medium specifications [4]

Our simulation settings involved setting spatial grid spacing at $\lambda/5 = 0.154\ \mathrm{mm}$ and temporal sampling frequency at 80 MHz. With this we generate raw RF datasets of size 128 x 6592 in the (x, t) domain.

The raw data set is preprocessed by first applying an initial time offset to this raw dataset, followed by amplification using time gain compensation coefficient of 0.4 dB/cm- MHz and finally filtering the sensor data using a gaussian filter.

For depth migration we use migration step $\Delta z = \lambda/10 = 0.077\ \mathrm{mm}$. Our Fourier domain grid size is $2^8 \times 2^{13}$ [4].

B. Overview of the Phase-Shift Depth Migration Method

Let $P(x, z, t)$ denote a two-dimensional scalar wavefield at time t and $v_z = c_z/2$ is the one way propagation velocity under Exploder Reflector Model Assumptions [4] .

Step 1: Compute $\psi(k_x, 0, f)$ by applying Fourier transform to $P(x, 0, t)$. Set $z^* \leftarrow 0$ and initialize $\psi(k_x, z^*, f) \leftarrow \psi(k_x, 0, f)$.

Step 2: Set $\psi(k_x, z^*, f) \leftarrow 0$ whenever $f^2 \leq {c_z}^2 {k_x}^2$. This is to exclude the evanescent wavefield region. Compute $\psi(k_x, z^* + \Delta z, f)$.

Step 3: Sum $\psi(k_x, z^* + \Delta z, f)$ along f axis and then apply inverse Fourier transform along the k_x axis to produce $\psi(x, z^* + \Delta z, 0)$. If the desired depth is not reached set $z^* \leftarrow z^* + \Delta z$ and repeat from step 2.

C. Overview of Compressive Sensing for Ultrasound Imaging

Let $f(t)$ be a signal with bandwidth $B > 0$. Then the Shannon-Nyquist sampling theorem says that to perfectly reconstruct this signal from its samples we need to sample it at the Nyquist rate, equal to twice the bandwidth of the signal, i.e. $2B$, (Shannon 1949; Nyquist 1928). Consider a real valued, finite length, one-dimensional, discrete time signal $\mathbf{x} \in R^n$. The claim of compressive sensing is that from m measurements where $m \ll n$, we can often perfectly reconstruct the original signal $\mathbf{x}$ where the measurements are not chosen in an adaptive manner.

Let $\{\psi_i\}_{i=1}^n$ be a set of n orthonormal basis vectors for the space R^n and let $\boldsymbol{\psi}$ be orthonormal matrix also known as the sensing matrix where the i^{th} column is the i^{th} basis vector ψ_i. Hence, we can express any signal $\mathbf{x} \in R^n$ as a linear combination of these basis vectors by

$$\mathbf{x} = \sum_{i=1}^{n} z_i \psi_i = \boldsymbol{\psi}\mathbf{z} \quad (1)$$

Where $\mathbf{z} \in R^n$ is the vector of inner products $z_i = \langle \mathbf{x}, \psi_i \rangle$.

The two vectors $\mathbf{x}$ and $\mathbf{z}$ are equivalent representations of the same signal. Typically, we say that $\mathbf{x}$ is in the time domain (if it is a time dependent signal, such as audio) or in the spatial domain if it is a spatially dependent signal, such as an image and we say that $\mathbf{z}$ is in the $\boldsymbol{\psi}$ domain. We measure the signal x by sampling it with respect to a a measurement matrix $\boldsymbol{\Phi} \in R^{m \times n}$. Let $\boldsymbol{\Phi}$ have rows Φ_i for $1 \leq i \leq m$. Each observation y_i corresponds to the inner product $y_i = \langle \Phi_i, \mathbf{x} \rangle$. Writing this in matrix-vector notation we get $\mathbf{y} = \boldsymbol{\Phi}\mathbf{x}$. It is evident that if $m \geq n$ and the rows of Φ span R^n we can achieve a perfect reconstruction of vector $\mathbf{x}$ from its observations $\mathbf{y}$.

Hence, we can write y as

$$\mathbf{y} = \boldsymbol{\Phi}\mathbf{x} = \boldsymbol{\Phi}\boldsymbol{\psi}\mathbf{z} = \boldsymbol{\Theta}\mathbf{z} \quad \text{where } \boldsymbol{\Theta} = \boldsymbol{\Phi}\boldsymbol{\psi} . \quad (2)$$

We assume that $\mathbf{z}$ is s sparse i.e. it is a linear combination of only $s \ll n$ basis vectors. Hence now solving the equation for $\mathbf{z}$ is equivalent to solving the equation for $\mathbf{x}$ with $\boldsymbol{\psi}$ as the predetermined basis. It is required that $\boldsymbol{\phi}$ and $\boldsymbol{\Psi}$ are mutually incoherent (almost uncorrelated) to recover signal $\mathbf{x}$ with high probability. Selection of samples from signal $\mathbf{x}$ to create measurement vector $\mathbf{y}$ has to be done in a random manner (random under sampling). This randomness will create a noisy spectrum that will effectively reduce aliasing.

The goal of compressive sensing is to design a matrix $\boldsymbol{\Phi}$ and a reconstruction algorithm so that for s- sparse signals we require only small number of measurements $m \approx s$ or slightly larger. This doesn't violate the Shannon-Nyquist theorem since we are reconstructing only sparse signals. To design a good measurement matrix, it should not destroy the original signal contained in $\mathbf{x}$ which is not possible since the system is underdetermined. The measurement matrix should satisfy the restricted isometry property [9].

D. Optimization problem formulation

Candes et al. stated in their paper [10] that solving equation (2) is feasible through an optimization problem P0 that follows the l_0-minimization. For such a method to be applied, matrix has to have a specified isometry constant of the Restricted Isometry Property (RIP).

$$\text{P0:} \qquad \hat{\mathbf{z}} = \operatorname{argmin}_{\mathbf{z}\in R^n} \|\mathbf{z}\|_0 \ \text{ subject to } \ \mathbf{y} = \boldsymbol{\Theta}\mathbf{z} \tag{3}$$

where the l_0 pseudo-norm is: $\|\mathbf{z}\|_0 := |\{i, \mathbf{z_i} \neq 0\}|$

However, solving equation (3) is generally non-deterministic polynomial-time hard (NP hard), which means it would take a lot of time to solve such a problem and find the optimal solution (i.e the sparsest solution).

Another approach by Candes et al. [11] imposes more restriction on the full rank matrix $\boldsymbol{\Theta}$ (on its isometry constant to be exact) to solve the problem in equation (2). We can find the solution to (2) by solving problem P1 which is based on the Basis Pursuit algorithm (BP):

$$\text{P1:} \qquad \hat{\mathbf{z}} = \operatorname{argmin}_{\mathbf{z}\in R^n} \|\mathbf{z}\|_1 \ \text{ subject to } \ \mathbf{y} = \boldsymbol{\Theta}\mathbf{z} \tag{4}$$

where the l_1 norm is: $\|\mathbf{z}\|_1 = \sum_{i=1}^{n} |\mathbf{z_i}|$

E. <u>Scaled ADMM for compressive sensing</u>

The problem in (4) essentially deduces to solving the problem

$$\text{Minimize } \|\mathbf{z}\|_1 \tag{5}$$
$$\text{subject to: } \mathbf{y} = \boldsymbol{\Theta}\mathbf{z}$$

The above problem can be written as

$$\text{Minimize } \|\mathbf{z}\|_1 \tag{6}$$
$$\text{subject to: } C = \{\mathbf{z} : \ \boldsymbol{\Theta}\mathbf{z} = \mathbf{y}\}$$

which can be further written as

$$\text{Minimize } \|\mathbf{z}\|_1 + I_c(\mathbf{z}) \tag{7}$$

Where $I_c(\mathbf{z})$ is an indicator function associated with set C :

$$I_c(\mathbf{z}) = \begin{cases} 0 \ \text{if } \mathbf{z} \in C \\ +\infty \ \text{otherwise} \end{cases}$$

The above problem can now be written as

$$\text{Minimize } \|\mathbf{z}\|_1 + I_c(\mathbf{w}) \tag{8}$$
$$\text{subject to: } \mathbf{z} - \mathbf{w} = \mathbf{0}$$

The scaled ADMM iterations for the above problem can be given as

$$\mathbf{z}_{k+1} = \underset{\mathbf{z}}{\operatorname{argmin}} \left[\|\mathbf{z}\|_1 + \frac{\alpha}{2} \|\mathbf{z} - \mathbf{w}_k + \mathbf{v}_k\|_2^2 \right] \tag{9}$$

$$\mathbf{w}_{k+1} = \underset{\mathbf{w}}{\operatorname{argmin}} \left[I_c(\mathbf{w}) + \frac{\alpha}{2} \|\mathbf{w} - (\mathbf{z}_{k+1} + \mathbf{v}_k)\|_2^2 \right] = P_c(\mathbf{z}_{k+1} + \mathbf{v}_k)$$

$$\mathbf{v}_{k+1} = \mathbf{v}_k + \mathbf{z}_{k+1} - \mathbf{w}_{k+1}$$

where $P_c(\mathbf{z}_{k+1} + \mathbf{v}_k)$ is the projection of $(\mathbf{z}_{k+1} + \mathbf{v}_k)$ on set C.

The z-minimization step can be performed as

$$\mathbf{z}_{k+1} = S_{1/\alpha}(\mathbf{w}_k - \mathbf{v}_k) \tag{10}$$

Where operator S is defined by

$$S_{\partial}(z) \triangleq \text{sign}(z).\max\{|\mathbf{z}| - \partial, \mathbf{0}\}$$

Here operators sign , max and $|\mathbf{z}| - \partial$ are performed component wisely

The w- minimization step can be performed as solving a simple QP problem

$$\text{Minimize } \|\mathbf{w} - (\mathbf{z}_{k+1} + \mathbf{v}_k)\|_2 \tag{11}$$

$$\text{subject to: } \mathbf{y} = \boldsymbol{\Theta}\mathbf{w}$$

$$\therefore \mathbf{w}_{k+1} = \boldsymbol{\Theta}^{+}\mathbf{y} + \mathbf{P}_{\boldsymbol{\Theta}}(\mathbf{z}_{k+1} + \mathbf{v}_k)$$

Where $\boldsymbol{\Theta}^{+} = \boldsymbol{\Theta}^{\mathbf{T}}(\boldsymbol{\Theta}\boldsymbol{\Theta}^{\mathbf{T}})^{-1}$ and $\mathbf{P}_{\boldsymbol{\Theta}} = \mathbf{I} - \boldsymbol{\Theta}^{\mathbf{T}}(\boldsymbol{\Theta}\boldsymbol{\Theta}^{\mathbf{T}})^{-1}\boldsymbol{\Theta}$

So, the scaled ADMM iterations are given by

$$\mathbf{z}_{k+1} = S_{1/\alpha}(\mathbf{w}_k - \mathbf{v}_k) \tag{12}$$

$$\mathbf{w}_{k+1} = \boldsymbol{\Theta}^{+}\mathbf{y} + \mathbf{P}_{\boldsymbol{\Theta}}(\mathbf{z}_{k+1} + \mathbf{v}_k)$$

$$\mathbf{v}_{k+1} = \mathbf{v}_k + \mathbf{z}_{k+1} - \mathbf{w}_{k+1}$$

The scaled ADMM algorithm is as follows

Step 1: Input parameters $\alpha > 0$, $\mathbf{w}_0$, $\mathbf{v}_0$ and tolerance ϵ_p , ϵ_d. Set $k = 0$

Step 2: Compute $\mathbf{z}_{k+1}$, $\mathbf{w}_{k+1}$ and $\mathbf{v}_{k+1}$ using (14).

Step 3: Compute $\mathbf{r}_k = \mathbf{z}_{k+1}$ - $\mathbf{w}_{k+1}$ and $\mathbf{d}_k = \boldsymbol{\Theta}(\mathbf{w}_{k+1}$ - $\mathbf{w}_k)$

Step 4: If conditions $\|\mathbf{r_k}\|_2 < \epsilon_p$ and $\|\mathbf{d_k}\|_2 < \epsilon_d$ are satisfied output ($\mathbf{z_{k+1}}$, $\mathbf{w_{k+1}}$) as solution and stop otherwise set $k = k + 1$ and continue [12].

F. Proposed Method

Our proposed method involves usage of compressive sensing for compressive sampling over two dimensions. First compressive sensing is applied in in spatial domain to reduce the number of transducer elements with the aim of reducing hardware complexity and then compressive sensing is applied temporal domain to reduce the sampling rate during signal acquisition .

Let us denote $\mathbf{X} \in R^{N \times J}$ as our processed sensor data where

N = number of samples = 6592
J = number of transducer elements = 128

The sensor data is formed by J signals each of length N denoted by $\mathbf{x_1 x_2} \ldots\ldots\ldots\ldots\ldots \mathbf{x_J}$ Hence our $\boldsymbol{\psi}$ domain 1 D signals will be denoted by $\mathbf{z_j} \in R^n$ for i running from 1 to J [1].

$$\mathbf{z_j} = \boldsymbol{\psi}^{-1}\mathbf{x_j} \quad j \in \{1,2, \ldots\ldots J\} \tag{13}$$

The J signals from sensors are jointly s- sparse in the 1D $\boldsymbol{\psi}$ domain which means all $\mathbf{z_j}$ have s non-zero elements at unknown positions but different in values

We have two choices for our sensing basis $\boldsymbol{\psi}$. We can either use the inverse DFT matrix or the inverse DCT matrix as our sensing basis. Hence, we can write (1) as

$$\mathbf{x}_j = \boldsymbol{\psi}\mathbf{z}_j \; j \in \{1,2, \ldots\ldots J\} \tag{14}$$

We randomly decimate each $\mathbf{x_j}$ to get our measurements $\mathbf{y_j}$ .Hence our measurement matrix $\boldsymbol{\Phi} \in R^{M \times N}$is a matrix obtained by taking randomly M lines from an identity matrix of size $N \times N$

$$\mathbf{y}_j = \boldsymbol{\Phi}\mathbf{x}_j \; j \in \{1,2, \ldots\ldots J\} \tag{15}$$

Hence, we can now write $\mathbf{y}_j$ as

$$\mathbf{y}_j = \boldsymbol{\Phi\psi}\mathbf{z}_j = \boldsymbol{\Theta}\mathbf{z}_j \; j \in \{1,2, \ldots\ldots J\} \tag{16}$$

Which is same as (2)

Hence our proposed method is as follows.

I) Compressive sensing in spatial domain

1. Initialize number of transducer elements M
2. Generate the inverse DFT/DCT matrix $\boldsymbol{\psi}$ of size $\mathrm{J} \times \mathrm{J}$
3. Generate an identity matrix I of size $\mathrm{J} \times \mathrm{J}$ and Generate the measurement matrix $\boldsymbol{\Phi}$ by randomly taking M lines from this identity matrix.
4. Generate the vectors $\mathbf{y_n}$ by randomly decimating each $\mathbf{x_n}$.
5. Generate matrix $\boldsymbol{\Theta} = \boldsymbol{\Phi\psi}$
6. Apply scaled ADMM iterations as in section E to obtain $\mathbf{z_n}$
7. Obtain $\mathbf{x_n}$ by taking inverse DFT/DCT transform of $\mathbf{z_n}$.
8. Obtain the sensor data X by combining all $\mathbf{x_n}$.

II) Compressive sensing in temporal domain

1. Initialize number of measurements M
2. Generate the sensing matrix $\boldsymbol{\psi}$ as inverse DFT/DCT matrix of size $\mathrm{N} \times \mathrm{N}$
3. Generate an identity matrix I of size $\mathrm{N} \times \mathrm{N}$ and Generate the measurement matrix $\boldsymbol{\Phi}$ by randomly taking M lines from this identity matrix.
4. Generate the vectors $\mathbf{y_j}$ by randomly decimating each $\mathbf{x_j}$.
5. Generate matrix $\boldsymbol{\Theta} = \boldsymbol{\Phi\psi}$
6. Apply scaled ADMM iterations as in section E to obtain $\mathbf{z_j}$
7. Obtain $\mathbf{x_j}$ by taking inverse DFT/DCT transform of $\mathbf{z_j}$.
8. Obtain the sensor data X by combining all $\mathbf{x_j}$.

III. Results and Discussion

A. Simulation Results

We first used the scaled ADMM algorithm on a single measurement vector $\mathbf{y}$ to evaluate the convergence of the algorithm. It was observed that the residuals converge before 5 iterations of ADMM for every vector y. The plot of the residuals are shown below

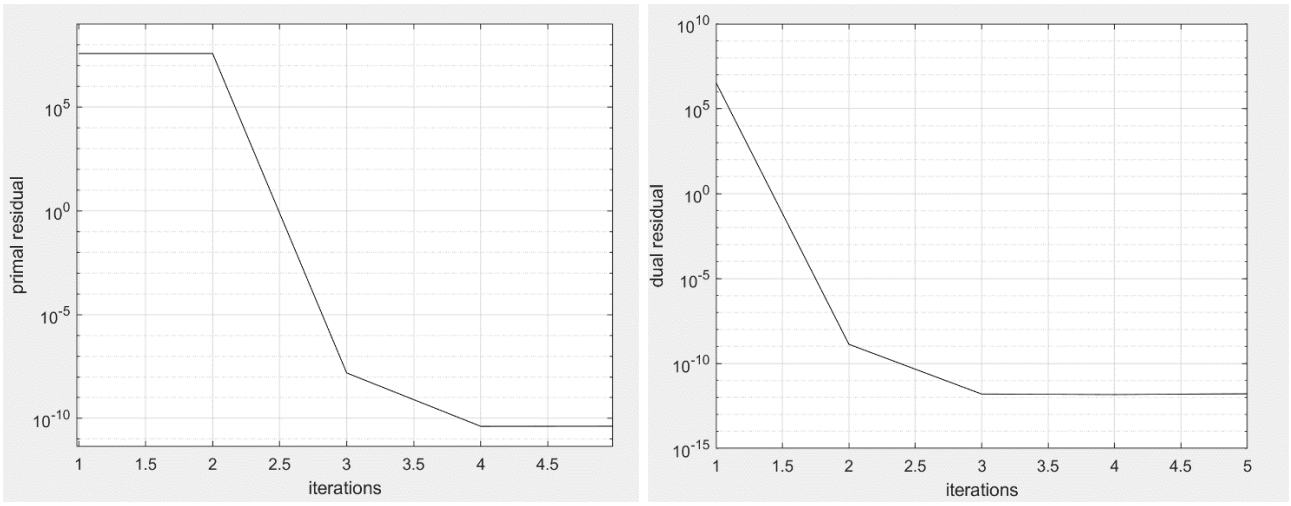

a) b)

Figure 1. a) Primal and b) Dual Residuals for the problem

a) Original Image

The original plots and original cross section of targets are shown below

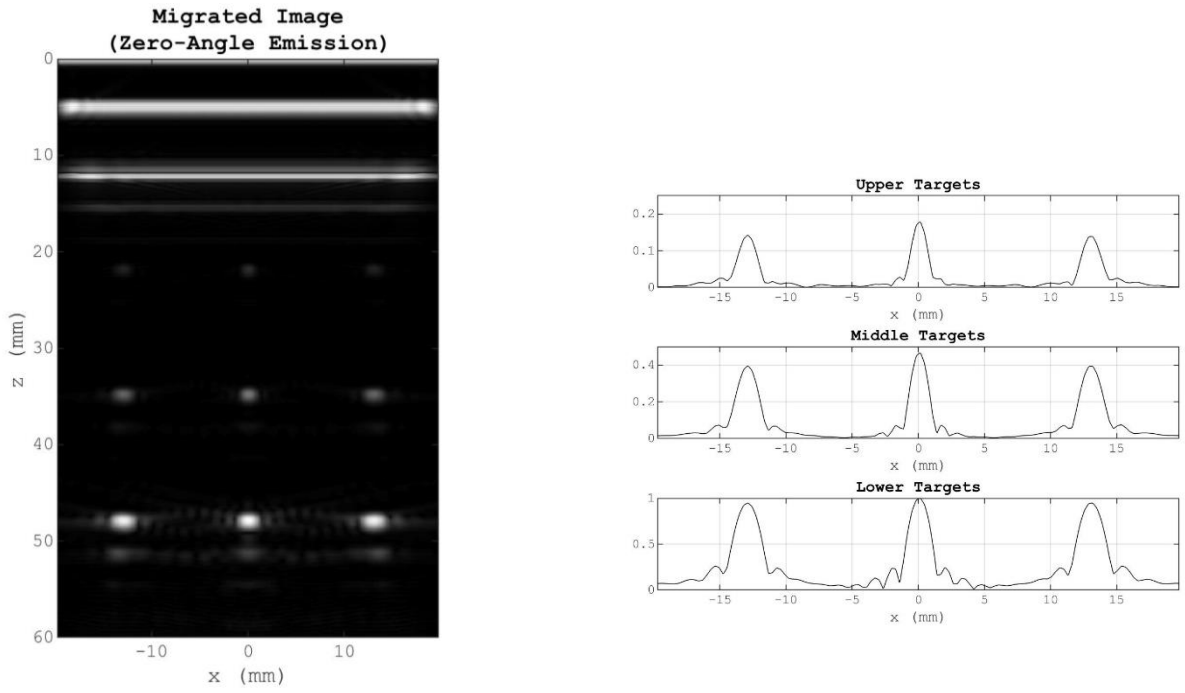

a) b)

Figure 2. a) Original Image From PW emission b) Cross section of imaging targets in the original image

FWHM in mm (zero angle):				
Upper Targets	[z = 21.791]:	L = 1.682	C = 1.405	R = 1.719
Middle Targets	[z = 34.727]:	L = 1.989	C = 1.613	R = 2.015
Lower Targets	[z = 47.817]:	L = 2.407	C = 2.034	R = 2.426

Table 3. Resolution Quality for the original Image

b) Spatial recovery with 25% of transducer elements (J = 32)

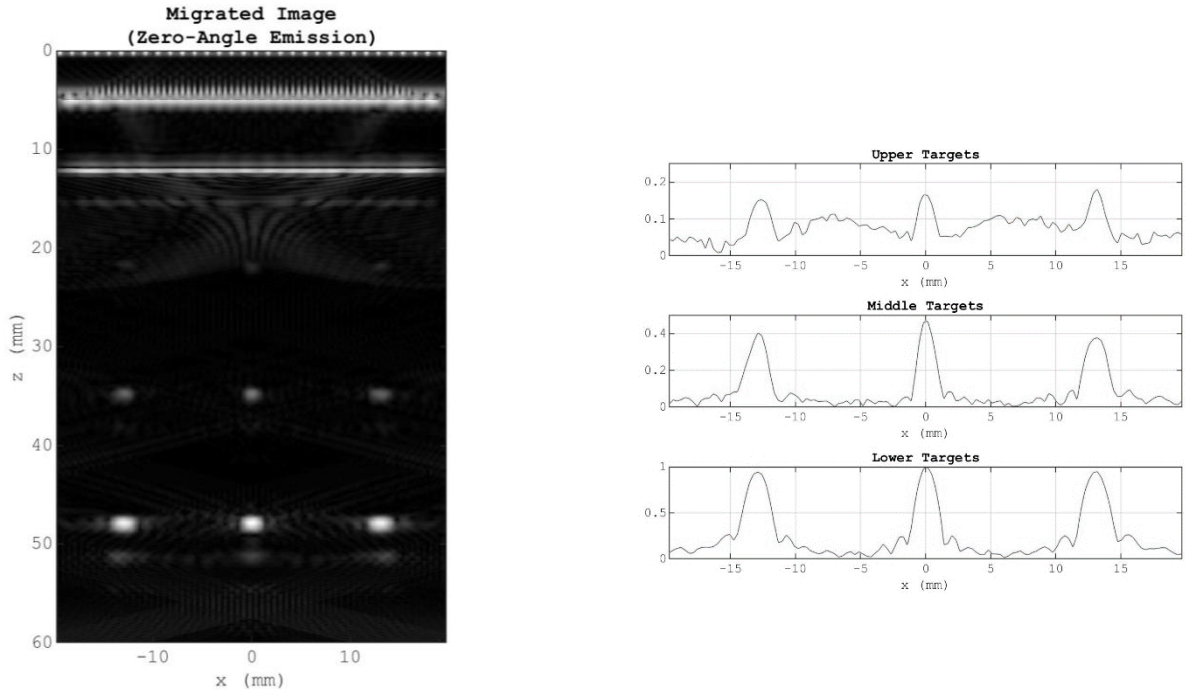

a) b)

Figure 3. a) Spatial recovery (J = 32) b) Cross section of imaging targets in Spatial recovery (J = 32)

FWHM in mm (zero angle):				
Upper Targets	[z = 21.791]:	L = 2.020	C = 1.661	R = 1.816
Middle Targets	[z = 34.804]:	L = 1.927	C = 1.591	R = 2.117
Lower Targets	[z = 47.894]:	L = 2.387	C = 2.052	R = 2.442

Table 4. Resolution Quality for Spatial recovery (J = 32)

c) Spatial recovery with 50% of transducer elements (J = 64)

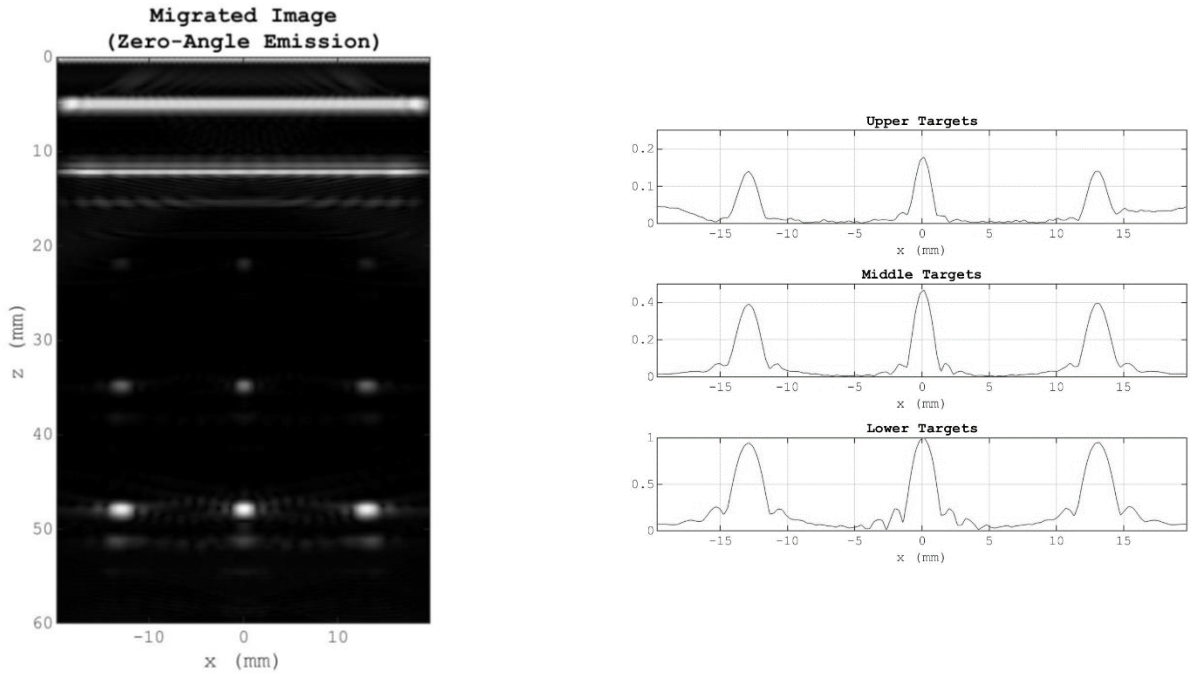

a) b)

Figure 4. a) Spatial recovery (J = 64) b) Cross section of imaging targets in Spatial recovery (J = 64)

FWHM in mm (zero angle):				
Upper Targets	[z = 21.791]:	L = 1.716	C = 1.400	R = 1.693
Middle Targets	[z = 34.727]:	L = 1.998	C = 1.612	R = 2.005
Lower Targets	[z = 47.817]:	L = 2.415	C = 2.024	R = 2.415

Table 5. Resolution Quality for Spatial recovery (J = 32)

d) Temporal recovery with 53% samples (N = 3500)

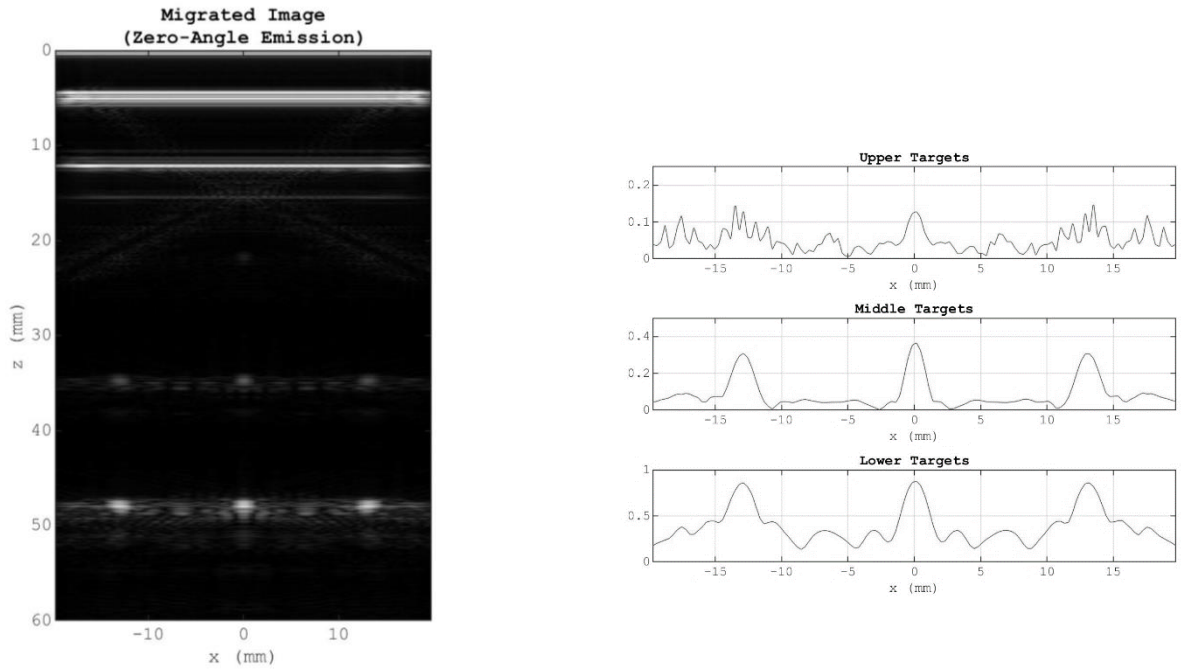

a) b)

Figure 5. a) Temporal recovery (N = 3500) b) Cross section of imaging targets in Temporal recovery (N = 3500)

FWHM in mm (zero angle):				
Upper Targets	[z = 21.945]:	L = 1.127	C = 1.610	R = 1.095
Middle Targets	[z = 34.804]:	L = 2.081	C = 1.702	R = 2.114
Lower Targets	[z = 47.971]:	L = 3.290	C = 2.537	R = 4.251

Table 6. Resolution Quality for Temporal recovery (N = 3500)

e) Temporal recovery with 83% of samples (N = 5500)

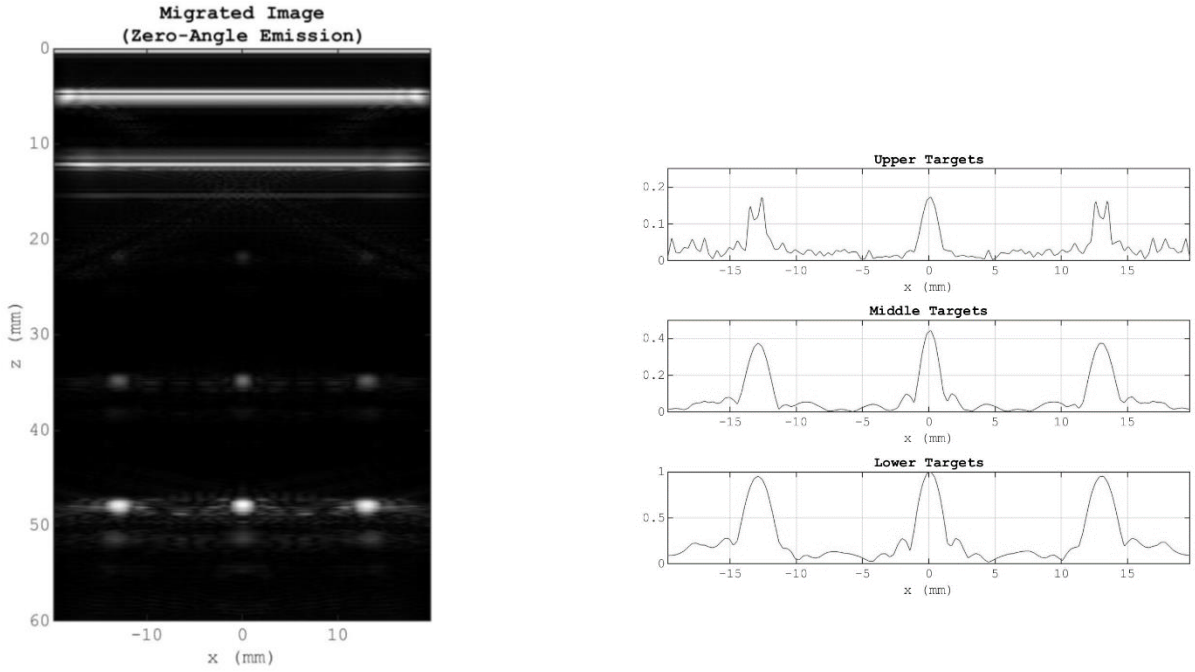

a) b)

Figure 6. a) Temporal recovery (N = 5500) b) Cross section of imaging targets in Temporal recovery (N = 5500)

FWHM in mm (zero angle):				
Upper Targets	[z = 21.791]:	L = 1.387	C = 1.474	R = 1.394
Middle Targets	[z = 34.804]:	L = 1.955	C = 1.576	R = 1.981
Lower Targets	[z = 47.894]:	L = 2.435	C = 2.096	R = 2.455

Table 7. Resolution Quality for Temporal recovery (N = 5500)

f) Spatial and Temporal recovery with J = 32, N = 3500

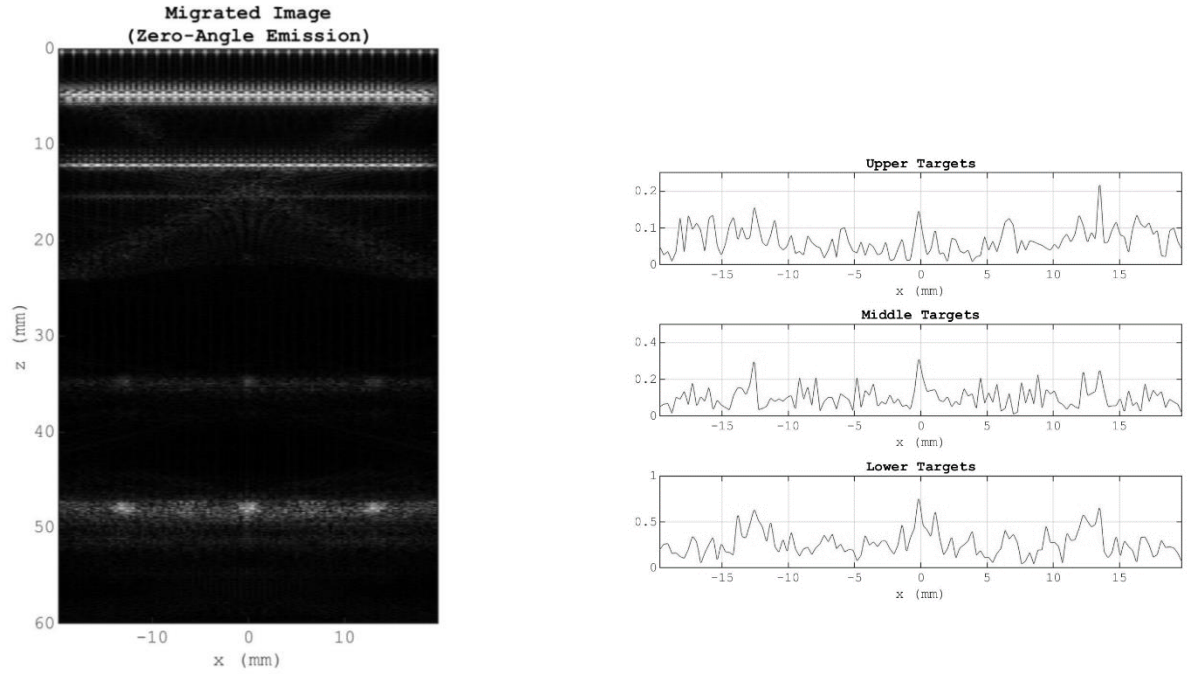

Figure 7. a) Spatial and Temporal recovery (J = 32, N = 3500) b) Cross section of imaging targets in Spatial and Temporal recovery (J = 32, N = 3500)

FWHM in mm (zero angle):				
Upper Targets	[z = 21.945]:	L = 0.836	C = 0.708	R = 0.473
Middle Targets	[z = 34.727]:	L = 0.649	C = 0.824	R = 1.002
Lower Targets	[z = 48.279]:	L = 2.312	C = 1.277	R = 2.052

Table 8. Resolution Quality for Spatial and Temporal recovery (J = 32, N = 3500)

g) Spatial and Temporal recovery with J = 64, N = 5500

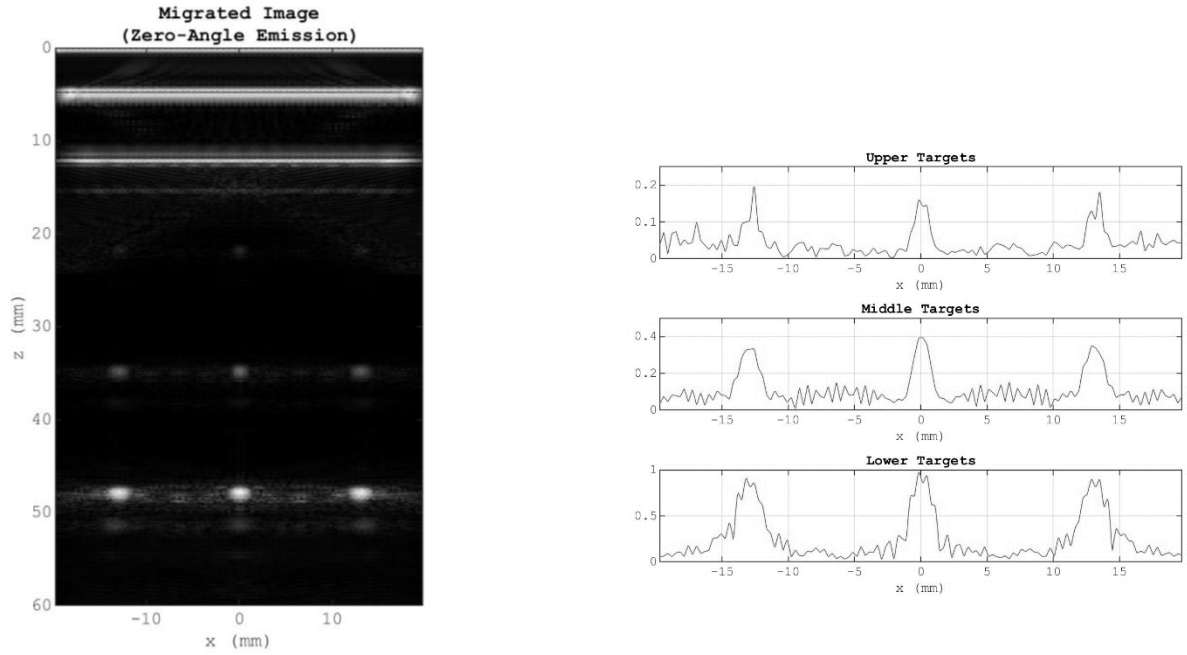

a) b)

Figure 8. a) Spatial and Temporal recovery (J = 64, N = 5500) b) Cross section of imaging targets in Spatial and Temporal recovery (J = 64, N = 5500)

FWHM in mm (zero angle):				
Upper Targets	[z = 21.791]:	L = 1.077	C = 1.393	R = 1.284
Middle Targets	[z = 34.573]:	L = 2.158	C = 1.624	R = 1.935
Lower Targets	[z = 47.663]:	L = 2.275	C = 2.136	R = 2.349

Table 9. Resolution Quality for Spatial and Temporal recovery (J = 64, N = 5500)

B. Analysis

We performed simulations using two different types of sensing basis, the inverse discrete Fourier transform matrix and the inverse discrete cosine transform matrix. The Average CPU time was calculated on an Intel® Core ™ i7-6500U CPU @ 2.5 GHz. It was found that the on an average simulations using inverse DCT as our sensing basis was approximately 70% faster than using inverse DFT. The results of the simulations remained the same. This is also evident from a theoretical perspective.

The recovered images are shown along with cross section of targets and FWHM values. The full width half maximum (FWHM) is used to measure the extent of the cross section. Lower the

peak values better is the resolution. Percentage improvement (+) and degradation (-) in target image quality with respect to the original image is shown below.

Experiment	J = 32	J = 64	N = 3500	N = 5500	J = 32, N = 3500	J = 64, N = 5500
Overall	-4%	+0.5%	-12%	+3.2%	+71% *	+6.5%
Upper	-12.5%	0%	+25.4%	+12.9%	+138%	+28%
Middle	-0.3%	0%	+4.7%	+1.9%	+127%	-1.8%
Lower	-0.2%	+0.2%	-31.8%	- 1.7%	+21.7%	-1.5%
Left	-4%	-0.8%	-6.5%	+5.2%	+10.3%	+10.3%
Center	-4.7%	+0.3%	-13.6%	-1.8%	+79.9%	-1.9%
Right	-3.4%	+0.7%	-17.4%	+5.6%	+74.6%	+10.6%

Table 10. Percentage Target Resolution Quality of the CS recovered images with respect to original image.

The target resolution quality results for J =32, N = 3500 (shaded column) when compared with its cross section and recovered image shows that it is a false positive. The same goes for upper targets in case of experiment with N = 3500(shaded cells). In these cases, we couldn't identify the targets due to distortion i.e. peaks are distorted in the cross section.

Subjectively we can say that experiments with J = 64 and J=64, N = 5500 yields a better recovery as compared to other simulation experiments.

IV. Conclusion

In this project we have implemented the compressive sensing technique to recover a sparse Ultrasound Image. The theory of Compressive Sensing is applied in two ways: in time domain and in spatial domain. Performance of both the individual approaches and their combinations were evaluated using several experiments. The recovery algorithm of scaled ADMM has fast convergence rate and low complexity. The spatially domain compressive sensing results for our application are better than temporal domain results while compressive sensing in both the domains yields fairly good results provided appropriate samples and elements are chosen.

V. References

[1] A. Basarab, H. Liebgott, O. Bernard, D. Friboulet and D. Kouamé, "Medical ultrasound image reconstruction using distributed compressive sampling," *2013 IEEE 10th International Symposium on Biomedical Imaging*, San Francisco, CA, 2013, pp. 628-631.

[2] M. Tanter and M. Fink, "Ultrafast imaging in biomedical ultrasound," *IEEE Trans. Ultrasonics, Ferroelectrics, and Frequency Control*, vol. 61, no. 1, pp. 102–119, Jan 2014.

[3] M. Albulayli , " Migration-Based Image Reconstruction Methods for Plane-Wave Ultrasound Imaging," Ph.D. dissertation, Department of Electrical and Computer Engineering, University of Victoria, Victoria, British Columbia, Canada , 2018.

[4] M.Albulayli and D. Rakhmatov, "Phase-Shift Depth Migration for Plane-Wave Ultrasound Imaging," *2018 40th Annual International Conference of the IEEE Engineering in Medicine and Biology Society (EMBC)*, Honolulu, HI, 2018, pp. 911-916.

[5] T. Blumensath, M.E. Davies, "Iterative hard thresholding for compressed sensing," Applied and Computational Harmonic Analysis, Volume 27, Issue 3, November 2009, Pages 265-274.

[6] C. Quinsac, A. Basarab, D. Kouamé and J. Grégoire, "3D Compressed sensing ultrasound imaging," *2010 IEEE International Ultrasonics Symposium*, San Diego, CA, 2010, pp. 363-366.

[7] M. Lustig, D. L. Donoho, J. M. Santos and J. M. Pauly, "Compressed Sensing MRI," in *IEEE Signal Processing Magazine*, vol. 25, no. 2, pp. 72-82, March 2008.

[8] http://www.k-wave.org/documentation/k-wave_ultrasound_simulation.php

[9] G.Pope ,"Compressive Sensing : A summary of Reconstruction Algorithms," Masters Thesis, Department of Computer Science, ETH Zurich, Switzerland, 2009 .

[10] E. J. Candes, J. Romberg and T. Tao, "Robust uncertainty principles: exact signal reconstruction from highly incomplete frequency information," in *IEEE Transactions on Information Theory*, vol. 52, no. 2, pp. 489-509, Feb. 2006.

[11] E. J. Candès, "The restricted isometry property and its implications for compressed sensing," *Comptes Rendus Mathematique*, vol. 346, no. 9–10, pp. 589–592, May 2008.

[12] W.S. Lu, "ECE573 Course Notes", Department of Electrical and Computer Engineering , University of Victoria, 2019.